Soft Matter

Accepted Manuscript

This is an *Accepted Manuscript*, which has been through the Royal Society of Chemistry peer review process and has been accepted for publication.

Accepted Manuscripts are published online shortly after acceptance, before technical editing, formatting and proof reading. Using this free service, authors can make their results available to the community, in citable form, before we publish the edited article. We will replace this *Accepted Manuscript* with the edited and formatted *Advance Article* as soon as it is available.

You can find more information about *Accepted Manuscripts* in the Information for Authors.

Please note that technical editing may introduce minor changes to the text and/or graphics, which may alter content. The journal's standard Terms & Conditions and the Ethical guidelines still apply. In no event shall the Royal Society of Chemistry be held responsible for any errors or omissions in this *Accepted Manuscript* or any consequences arising from the use of any information it contains.

ROYAL SOCIETY OF CHEMISTRY

www.rsc.org/softmatter

The Twisted Tauopathies: Surface Interactions of Helically Patterned Filaments Seen in Alzheimer's Disease and Elsewhere

Nash D. Rochman

Department of Chemical and Biomolecular Engineering, Johns Hopkins University

Sean X. Sun*

Departments of Mechanical and Biomedical Engineering, Johns Hopkins University, Baltimore MD 21218

Abstract

This paper broadly examines the dynamics of helically patterned filaments interacting with a surface and focuses on the surface interaction of amyloid fibrils formed by tau protein. Two structures are addressed in detail: cylindrical filaments with periodic thinning (CF-PT) and paired helical filaments (PHF). PHF is observed in neural tissue affected by Alzheimer's disease and may aggregate to form the pathological neurofibrillary tangles associated with the illness. Work in electron microscopy has demonstrated the conversion of CF-PT into PHF *in vitro*, suggesting CF-PT to be a PHF precursor *in vivo*. Here we model CF-PT as a patterned elastic rod placed on a flat surface (characteristic of the environment during microscopy) and examine the conformational changes resulting in stable surface bonding. Analysis of this conformational space reveals structures resembling PHF and thus provides a mechanistic explanation of the CF-PT to PHF transition. We develop a general phase diagram of the filament conformation as a function of filament twist and bend rigidity. Results of this work also suggest that we can obtain desired filament conformations by patterning interactions between elastic filaments with a substrate, and therefore can be used as a method in microfabrication.

*Electronic address: ssun@jhu.edu

Soft Matter Accepted Manuscript

I. INTRODUCTION

Tauopathies are a group of diseases linked by the pathological aggregation of the tau protein. Tau is known to be a microtubule stabilizing protein prevalent in neurons of the central nervous system. Owing to this fact, many tauopathies are neurodegenerative disorders perhaps the most commonly discussed being Alzheimer's disease[1]. Beginning with the original characterization by Alois Alzheimer in 1907, great interest has been taken in the striking structural changes of affected neurons showing the accumulation of dense, tangled fiber bundles completely reshaping neural tissue[2]. Over time much improved imaging techniques have become available, and as great efforts have been taken to determine the composition of these tangles; increasingly finer structures have been elucidated encouraging the suggestion of detailed mechanisms of formation. In particular, recent developments in scanning transmission electron microscopy (STEM) have presented many striking images of the fine structure of individual, unbundled fibers. One such structure which may aggregate to form these tangles, and the primary concern of this discussion, is the paired helical filament (PHF) which has recently been realized to be an amyloid fibril formed by tau protein[3].

As the name suggests, PHF's were initially posited to be pairs of individual filaments twisted about one another[4], an explanation favored until electron microscopic data became available[5] which suggests PHF's to be single filament structures. In these images, another class of filament is often seen in regions occupied by PHF, namely cylindrical filaments with periodic thin regions (CF-PT) also labelled "straight filaments"[6]. CF-PT bears a close resemblance to PHF, sharing the same turn period; however, CF-PT has a smaller radial variance than PHF with larger thin regions and smaller wide regions. In addition, upon sonication, it has been observed that a mixed population of CF-PT and PHF is converted into one wholly composed of PHF[5]. Motivated by this information, Ruben et al. have suggested CF-PT to be a PHF precursor filament. It is a primary goal of this paper to provide a surface mediated mechanism for the conversion of CF-PT to PHF. Towards this aim, let us take a closer look at the fine structure of amyloid fibrils.

Utilizing the electron microscopic data discussed above in addition to solid state NMR, Paravastu et al. have suggested a structural model for amyloid fibrils where each fiber is composed of a series of triangular sheets subject to an intrinsic twist along the fibril axis (see Figure 1 a.)[7]. In the next section, we will consider the Paravastu model to be the

Soft Matter Accepted Manuscript

primary structure of each fibril and examine what secondary structures develop when fibrils are allowed to rest on a flat, attractive surface.

We will begin our investigation by working with a simplified, cylindrical model for the fibril and examine the system in terms of elastic bending and twisting energies, and bonding energies with the underlying surface. We use analytic theory to find preferred filament conformations resulting in stable bonding with the surface and thus restrict our analysis to a simple system where we assume isotropic bend stiffness. The general case, for filaments with anisotropic bend stiffness, has been studied recently [8] presenting a rich description of the possible conformational states. Here, with our simpler model, we cannot recreate all the conformations presented in that work, but instead focus on generating those with out-of-plane (writhing) configurations. With the exception of a single conformation (introduced as the "Unwound" filament below) we will be exclusively examining conformations which are kinetically-quenched with a fixed linking number. These problems fall under the general category of elastic filaments interacting with other objects. A prime example of this is the coiled coil structure encountered in proteins[9], which through helical bonding interaction between alpha-helical filaments, can form a variety of geometries[10–12] Others have examined conformations of filament bundles and ropes. These complex structures are formed by balancing mechanical deformation energy with bonding energy between filaments.

The theory developed for the fibril will then be reconsidered in the context of the Paravastu structure and we will provide a surface mediated mechanism for the conversion of CF-PT to PHF identifying CF-PT as a non-bending Paravastu fibril and PHF as its helical secondary structure. Before we begin construction of the model we first wish to state that, for simplicity, we assume the cylindrical filaments with helical bonding patterns (representing CF-PT) form free from the surface and make contact with the surface all at once. We recognize the limitations inherent to this assumption towards direct comparison with dynamic experimental data.

II. MODELING METHOD

Note that over the course of this discussion we will introduce parameters relevant to the description of the fibril. A summary of key parameters can be found in Table I (following Figure 5). The first thing we must do is motivate the substitution of cylinders for the

Soft Matter Accepted Manuscript

more detailed fibril structure. To do so, consider one period of the Paravastu structure and identify the edges of each triangular face that are closest to and thus most likely to bond with the surface. Each face has exactly one such edge apart from the face directly in the middle of the period (and completely inverted) which has two. If each face is replaced by a disc, and the identified edges become designated bonding points rotated about the axis of the filament by an angle equal to that of the original edge, we find that these points map the outer third of a helix with the "center" missing - that is the region where the pattern would lie primarily in the upper hemisphere of the cylinder with respect to the surface. If this region is primarily non-bonding, a fact which will be demonstrated below, a cylinder with a simple helical bonding region will well approximate the fibril structure. The greatest discrepancy is the fact that a full helix is represented by a twist of 2π over the turn length whereas the actual fibril structure twists by a total of $\frac{2\pi}{3}$; thus the preferred bonding state for the fibril will have less accumulated twist than the cylinder. This will be addressed later; for now, let us focus on the simplified case.

Here we will explore the dynamic conformation changes of helically patterned rods or filaments - that is cylinders with a helical bonding pattern on their surfaces. We will label the period of the helical pattern L and a filament segment of length L a "monomer" (see Figure 2). This bonding pattern will be able to stick to objects on which a filament is placed (for instance a flat plate) with a "close-contact" approximation depending on the nature of that object's surface. The filament will then twist along its longitudinal (or tangential) axis and bend along its radial axes to increase contact of the bonding pattern with the object while balancing the mechanical strain induced by this process. In particular, we will be discussing the case where the filament twists to increase bonding contact and bends to facilitate that twist. We will only consider filaments of total length mL where m is an integer number of monomers.

Our goal is to find the most stable geometries for these filaments when they are placed on a flat plate to which the bonding pattern can stick. Perhaps the most natural place to start will be with a general expression defining filament geometry and to show how one can derive the energy from that geometry. Beginning with a point in three dimensional space $\mathbf{p}_n$, and a coordinate frame (three orthonormal vectors $\mathbf{e}_1$,$\mathbf{e}_2$, and $\mathbf{e}_3$), one may trace out any space curve containing that point in the following way (noting that without a loss of generality, one may select $\mathbf{e}_3$ to be the tangent vector of the filament at the selected point)

Soft Matter Accepted Manuscript

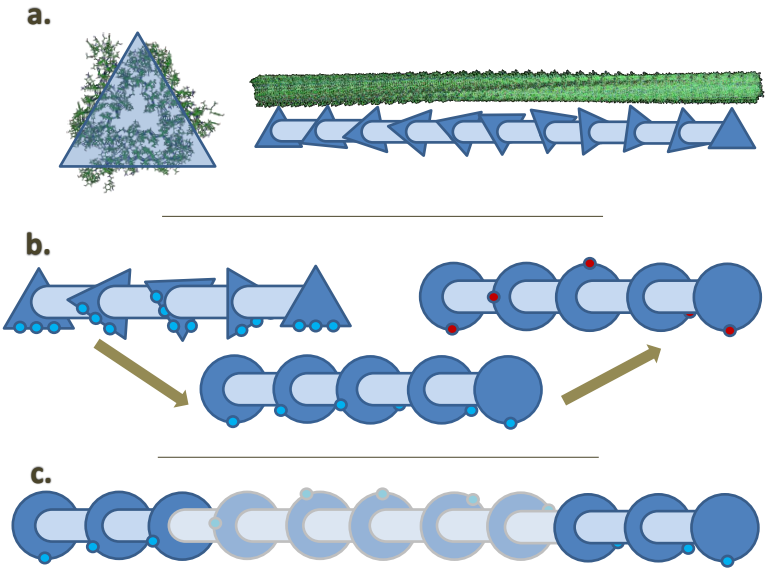

Figure 1: a. Overlay of the molecular structure constructed using the atomic coordinates published online[7] (PDB ID: 2LMP) in the Protein Data Bank[13] with our graphical representation. The lighter blue cylinders are regions where the triangular faces are omitted to better represent the twist over the length of the fibril. b. Motivation for the simplified fibril representation in two steps: first, identification of each face as a disc with a single bonding point replacing the edge of each face closest to the surface; second, the continuation of the resultant helical bonding pattern. c. Visualization of the section of the bonding pattern missing from the actual filament.

with index n: pick three angles, $\theta_1(n-1)$,$\theta_2(n-1)$, and $\theta_3(n-1)$; rotate $\mathbf{e}_1(n-1)$,$\mathbf{e}_2(n-1)$, and $\mathbf{e}_3(n-1)$ by angles $\theta_1(n-1)$,$\theta_2(n-1)$, and $\theta_3(n-1)$ about axes $\mathbf{e}_1(n-1)$,$\mathbf{e}_2(n-1)$, and $\mathbf{e}_3(n-1)$ respectively; pick the next point to be $\mathbf{p}_n = \mathbf{p}_{n-1} + S\mathbf{e}_3(n-1)$ where S is a real number; and repeat. It should be noted that θ_1,θ_2, and θ_3 must be sufficiently small so that the three dimensional rotations are commutative and the construction is well defined. This can be ensured by converting this discrete construction to a continuous one replacing the angles θ_i with angular velocities $\frac{d\theta_i}{ds}$ and defining the space curve in the following way with a general infinitesimal rotation matrix. Here $\mathbf{e_i}(s)$ is the solution to the equation:

$$\frac{d\mathbf{e}_i(s)}{dt} = \begin{bmatrix} 0 & \frac{d\theta_3}{ds} & \frac{-d\theta_2}{ds} \\ -\frac{d\theta_3}{ds} & 0 & \frac{d\theta_1}{ds} \\ \frac{d\theta_2}{ds} & \frac{-d\theta_i}{ds} & 0 \end{bmatrix} \mathbf{e}_i(s) \tag{1}$$

Soft Matter Accepted Manuscript

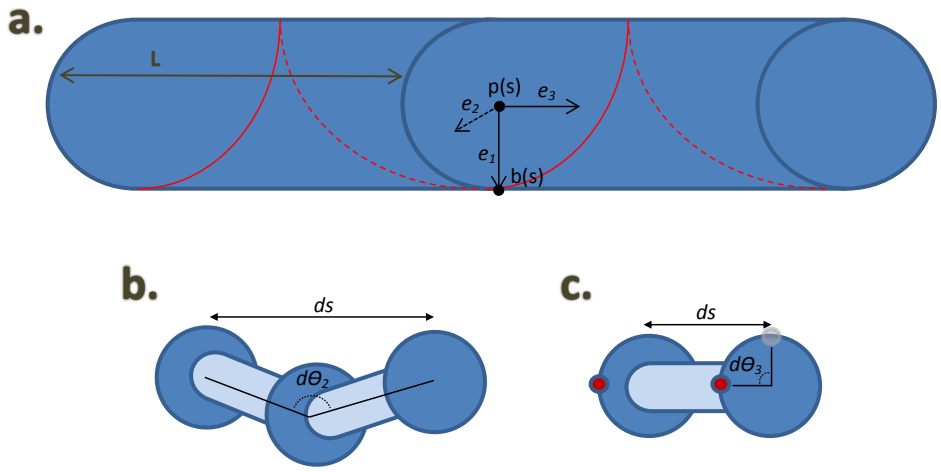

Figure 2: a. Two monomers overlaid with the coordinate axes defined at each point $p(s)$ of the center of the fibril: e_3, the unit vector tangent to the fibril; e_1, the unit vector in the direction of the bonding point $b(s)$; and e_2 defined to be e_1 cross e_3. b. An illustration of fibril bend along the e_2 axis, $\frac{d\theta_2}{ds}$. c. An illustration of fibril twist along the e_3 axis, $\frac{d\theta_3}{ds}$ – in this image the pattern appears in the same spot on both discs because the fibril was twisted: with no twist the bonding pattern on the right disc would have been where the grey dot is.

subject to the initial conditions $\mathbf{e}_i(0) = \mathbf{e}_i^0$, and $\mathbf{p}(s)$ is given by:

$$\mathbf{p}(s) = \mathbf{p}_0 + \int_0^s \mathbf{e}_3(s')ds' \tag{2}$$

For convenience, we'll choose $\mathbf{p}_0 = [0, 0, a]$ and $\mathbf{e}_i^0 = -\mathbf{e}_z, \mathbf{e}_x, \mathbf{e}_y$. $\mathbf{p}(s)$ specifies the point corresponding to the center of the slice (a disk) of the filament a length s down from $\mathbf{p}_0$. Now to define the bonding pattern $\mathbf{b}(s)$, we can label the radius of the filament a, and (again without a loss of generality) choose the bonding point such that $\mathbf{e}_1$is the radial vector satisfying $\mathbf{b}_0 = \mathbf{p}_0 + a\mathbf{e}_1(0)$. We can now prescribe a helical pattern in terms of, $\mathbf{e}_1(s)$, and $\mathbf{e}_2(s)$:

$$\mathbf{b}(s) = \mathbf{p}(s) + a\left[\cos\left(\frac{-2\pi}{L}s\right)\mathbf{e}_1(s) + \sin\left(\frac{-2\pi}{L}s\right)\mathbf{e}_2(s)\right] \tag{3}$$

Finally we can note $\mathbf{b}_0 = [0, 0, 0]$.

Equipped with the tools to define filament geometry, we can construct the formalism for the energy. Considering the elastic limit, the filament may be approximated to behave in a

Soft Matter Accepted Manuscript

springlike fashion such that the strain energy is a function of angular shift squared i.e.:

$$E_{Bend} = \kappa_B \int_0^{mL} \left(\frac{d\theta_1}{ds}\right)^2 + \left(\frac{d\theta_2}{ds}\right)^2 ds \tag{4}$$

$$E_{Twist} = \kappa_T \int_0^{mL} \left(\frac{d\theta_3}{ds}\right)^2 ds \tag{5}$$

where κ_B and κ_T are the elastic moduli for the bend and twist of the filament respectively - a measure of filament stiffness. There is one more term to consider - the bonding energy of the filament. Given a "contact" distance, ε, and the bonding energy with the flat plate per unit length, γ (< 0), we can fix the plate in the $x - y$ plane and write down a bonding function as follows:

$$G_{Bond}(s) = \begin{cases} 1 & \mathbf{B}(s)\cdot\mathbf{e}_z \leq \varepsilon \\ 0 & else \end{cases} \tag{6}$$

and the bonding energy:

$$E_{Bond} = \gamma \int_0^{mL} G_{Bond}(s) ds \tag{7}$$

Putting these three terms together, we get a general expression for filament energy:

$$E\left(\kappa_B, \kappa_T, \gamma, \frac{d\theta_i}{ds}(s)\right) = \int_0^{mL} \kappa_B \left[\left(\frac{d\theta_1}{ds}\right)^2 + \left(\frac{d\theta_2}{ds}\right)^2\right] + \kappa_T \left(\frac{d\theta_3}{ds}\right)^2 + \gamma G_{Bond}(s) ds \tag{8}$$

As clean as this construction may be, it is unfortunately quite difficult to ascertain $G_{Bond}(s)$ given an arbitrary form for $\frac{d\theta_i}{ds}(s)$. For this reason, we will start by trying to restrict the form of $\frac{d\theta_3}{ds}(s)$ in a way that will make the problem more tractable without losing any strongly bonded configurations. In addition we will take the limit $\varepsilon \to 0$ for close contact.

A. Selecting Relevant Conformations

Before we contiune, we would like to note again that we are focused primarily on kinetically-quenched structures where the linking-number is fixed. Let us consider three simple filament confirmations in contact with the surface. The first case is an unbent filament segment of length l which, before twisting, has one point of contact between its bonding pattern and the bonding surface. Further let $\frac{d\theta_3}{ds}(s) = c$ over this local region. If $c = 0$, the twist energy attains its minimum value of 0 and a finite number of points (one point) on the filament are bonded to the surface. The second case is when $-\infty < c < \frac{2\pi}{L}$

Soft Matter Accepted Manuscript

or $\frac{2\pi}{L} < c < \infty$. The twist energy is nonzero and still only a finite number of points on the filament can bind to the surface. The third case is when $c = \pm\frac{2\pi}{L}$, it is possible for **every** point of the bonding pattern to bond to the surface. Recalling, $E_{Bond} = \gamma \int_0^l G_{Bond}(s)ds$, and noting that $G_{Bond}(s)$ takes the form of a sum of finitely valued delta functions, in cases one and two we find the filament energies to be: $E_{Bond}^{First} = E_{Bond}^{Second} = 0$ and $E_{Bond}^{Third} < 0$; $E_{Twist}^{First} = 0$, E_{Twist}^{Second}, $E_{Twist}^{Third} > 0$. Thus we see that to find the minimum energy solution for the segment, c takes one of two possible magnitudes; for the limiting case of high κ_T, $c = 0$, otherwise $c = \frac{2\pi}{L}$. We can also see that if the same condition, $\frac{d\theta_3}{ds}(s) = c$, is imposed on an unbent segment, which has **no** points of contact between its bonding pattern and the surface before twisting, the bonding energy is zero. Thus we will restrict ourselves to considering $\frac{d\theta_3}{ds}(s)$ to be a piecewise constant function attaining the values $\pm\frac{2\pi}{L}$ or 0 over each segment depending on whether it is bonding or nonbonding (Note this requirement will be slightly relaxed later). Now we would like to find similar restrictions for $\frac{d\theta_1}{ds}(s)$ and $\frac{d\theta_2}{ds}(s)$. To do so, we will first need to discuss the coupling between filament bend and twist.

When a filament begins to strain to bond with the surface, as discussed above, every region around a point of contact between the bonding pattern and the surface may twist to increase the magnitude of the bonding energy; but regions without these contact points may not. For a filament of length mL there are $m+1$ such points. Different shapes develop depending on how many of these points initially twist. The two extreme cases corresponding to one point and all $m+1$ points initiating twist are depicted in the bottom and top of Fig. 3 respectively.

When twist initiates from a single point (Fig. 3b), maximal contact can be achieved by twisting; however, reaching this conformation requires all but one of the points initially bound to the surface to be temporarily lifted. This is a special case which will be referred to as an "unwound" filament and will be investigated in more detail later when a fuller energy landscape has been developed. On the other hand, when multiple points initiate twist (Fig. 3a.), the filament faces a geometric constraint that forces the introduction of a complementary bend or twist. This can be seen as follows: consider that two points p and q are initiating twist. In the region $[p, q]$, p initiates twist with an angular velocity of $-\frac{2\pi}{L}$and q initiates twist with an angular velocity of $\frac{2\pi}{L}$. If each twisted region is of length $\frac{\delta}{2}$, then the point $p + \frac{\delta}{2}$ is twisted by an angle of $\frac{2\pi\delta}{L}$ from the point $q - \frac{\delta}{2}$. Without allowing the filament to break, this requires that the region $[p + \frac{\delta}{2}, q - \frac{\delta}{2}]$ bend or twist by at least $\frac{2\pi\delta}{L}$.

Soft Matter Accepted Manuscript

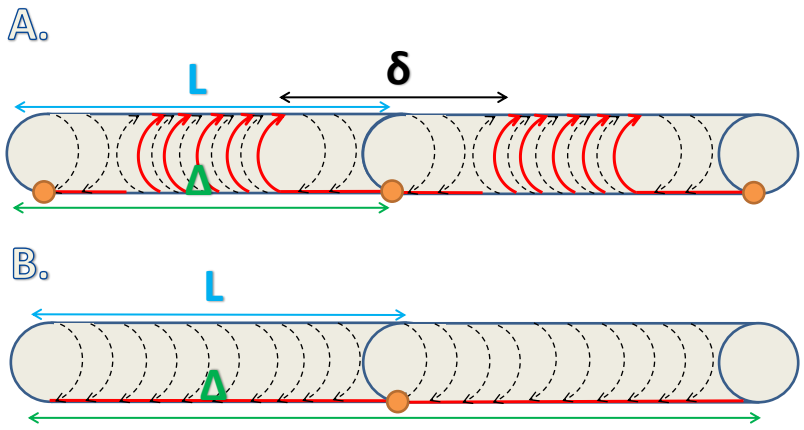

Figure 3: Depictions of the two types of filament bonding twist. On the bottom - single initial point. On the top - multiple. Here Δ specifies the period of physical twisting and L that of the bonding pattern.

We must also determine what types of bend are equivalent to twisting the filament. The basic problem statement is that we want to know what collections of rotations about $\mathbf{e}_1$ and $\mathbf{e}_2$ are equivalent to a single rotation about $\mathbf{e}_3$. One may quickly show (see Appendix A) that any rotation about $\mathbf{e}_3$ can be achieved by moving the plane formed by $\mathbf{e}_1$ and $\mathbf{e}_2$ into the plane normal to $\mathbf{e}_3$ and rotating about $\mathbf{e}_1$ by an equivalent angle. Additionally we can verify (see Appendix A) that any arbitrary rotation may be written as a rotation about only two axes (i.e. that combinations of bend deformations alone is equivalent to an arbitrary rotation of the coordinate frame). Before we go on, we may note that excepting the special case where the desired rotation about $\mathbf{e}_3$ is 2π which will be discussed below (as the "looped" case in the next section), the minimum number of rotations about $\mathbf{e}_1$ and $\mathbf{e}_2$ that can achieve the desired result is three. In short, to accomplish a net rotation about $\mathbf{e}_3$ by only rotating about $\mathbf{e}_1$ and $\mathbf{e}_2$ in this fashion, one must rotate an extra π radians about $\mathbf{e}_1$ or $\mathbf{e}_2$.

Finally we note that the lowest energy solution for a non-bonding region is also one of constant twist and bend. Note that we only consider regions that bend around either $\mathbf{e}_1$ or $\mathbf{e}_2$, but not both to ensure the boundary conditions are satisfied. Consider a non-bonding region of length l that must bend/twist by an angle ψ. We may write the angular velocity over this region as $\frac{d\theta_{i,j}}{ds} = \frac{\psi}{l} + f(s)$ such that integrating the angular velocity over the total

Soft Matter Accepted Manuscript

length yields ψ:

$$\int_0^l \frac{\psi}{l} + f(s)ds = \psi \Rightarrow \int_0^l f(s)ds = 0. \tag{9}$$

Integrating the square of the velocity over l yields the deformation energy (up to some multiplicative constant):

$$\int_0^l \left(\frac{\psi}{l} + f(s)\right)^2 ds = \frac{\psi^2}{l} + 2\frac{\psi}{l}\int_0^l f(s)ds + \int_0^l f^2(s)ds = \frac{\psi^2}{l} + \int_0^l f^2(s)ds \tag{10}$$

We see that the strain is minimized when $f(s) \equiv 0$ and the angular velocity is constant.

Now we have suitable restrictions on $\frac{d\theta_{i,j}}{ds}(s)$: between points bonded to the surface: they integrate to null (or $2\pi n$); they are piecewise constant; and over bonding regions $\left|\frac{d\theta_3}{ds}(s)\right| = \frac{2\pi}{L}$. These rules all lead to strongly bonded conformations. In particular let us look at the following class of filaments: considering a total length of mL, divide the filament into regions of length Δ such that:

$$\Delta = \frac{mL}{M} \tag{11}$$

where M is an integer (see Fig. 3). Now we may define $\frac{d\theta_i}{ds}(s)$ as follows. We want the strain to be constant over both regions that bend along $\mathbf{e}_2$, and those that bend along $\mathbf{e}_1$. According to Eq. (35), the total bend in $\mathbf{e}_2$ is of angle $d = \frac{2\pi\delta}{L}$ where δ is the length of the bonding region with the surface and the total bend in $\mathbf{e}_1$ is of angle $a + c = \pi$. Stated another way, this means that if l_i is the length of the non-bonding region over which $\mathbf{e}_i$ bends, then:

$$\frac{\pi}{l_1} = \frac{\left(\frac{2\pi\delta}{L}\right)}{l_2} \Rightarrow l_1 = \frac{L}{2\delta}l_2 \tag{12}$$

because the total angular velocity is constant as stated in Eq. (10). The total length of the non-bonding region is $\Delta - \delta = l_1 + l_2$, which yields:

$$l_1 + l_2 = \left(1 + \frac{L}{2\delta}\right) l_2 = \Delta - \delta \Rightarrow l_2 = \frac{\Delta - \delta}{\frac{L}{2\delta} + 1} \tag{13}$$

This specifies the following functions for our angular velocities:

$$\frac{d\theta_3}{ds}(s) = \begin{cases} \frac{2\pi}{L} & s \in [n\Delta, n\Delta + \frac{\delta}{2}] \cup [(n+1)\Delta - \frac{\delta}{2}, (n+1)\Delta] \\ 0 & else \end{cases} \tag{14}$$

$$\frac{d\theta_1}{ds}(s) = \begin{cases} \frac{2\pi\delta/L + \pi}{\Delta - \delta} & s \in [n\Delta + \frac{\delta}{2}, n\Delta + \frac{1}{2}(\Delta - l_2)] \cup [(n+1)\Delta - \frac{1}{2}(\Delta - l_2), (n+1)\Delta - \frac{\delta}{2}] \\ 0 & else \end{cases} \tag{15}$$

Soft Matter Accepted Manuscript

$$\frac{d\theta_2}{ds}(s) = \begin{cases} \frac{2\pi\delta/L+\pi}{\Delta-\delta} & s \in [n\Delta + \frac{1}{2}(\Delta - l_2), (n+1)\Delta - \frac{1}{2}(\Delta - l_2)] \\ 0 & else \end{cases} \tag{16}$$

where n is an integer between 0 and $M-1$, and $\delta < \Delta$. We can calculate the energies of filament configurations as follows:

$$E(\Delta,\delta) = M\left[\underbrace{\int_0^{\Delta-\delta} \kappa_B \left(\frac{2\pi\delta/L+\pi}{\Delta-\delta}\right)^2 ds}_{nonbondingregion} + \underbrace{\int_0^{\delta} \kappa_T \left(\frac{2\pi}{L}\right)^2 ds}_{bondingregion}\right] + \int_0^{mL} \gamma G_{Bond}(s) ds \tag{17}$$

We have restricted $\frac{d\theta_i}{ds}(s)$ so that we can write down the bonding term as

$$\int_0^{mL} \gamma G_{Bond}(s) ds = \frac{\gamma\delta}{2} \sum_{n=0}^{M} \sum_{\alpha=0}^{m} \Gamma(n,\alpha) \tag{18}$$

where:

$$\Gamma(n,\alpha) = \begin{cases} 2 & n\Delta = \alpha L,\ n \neq 0, M \\ 1 & n\Delta = \alpha L,\ n = 0, M \\ 0 & else \end{cases} \tag{19}$$

This function is merely restating that only regions around points of initial contact between the bonding pattern and the surface can initiate twist to increase bonding energy. Plugging this into Eq. (17) yields (the general form of the energy for the "helix" conformation in the next section):

$$E(\Delta,\delta) = M\left[\frac{\kappa_B}{\Delta-\delta}\left(\frac{2\pi\delta}{L}+\pi\right)^2 + \kappa_T\delta\left(\frac{2\pi}{L}\right)^2\right] + \frac{\gamma\delta}{2}\sum_{n=0}^{M}\sum_{\alpha=0}^{m}\Gamma(n,\alpha) \tag{20}$$

We can now explore the possibilities for Δ and find the optimal δ minimizing the energy (see Fig. 4). We see that the minimum energy configurations occur for Δ that meet the following condition:

$$N\Delta = mL \, where \, N \, is \, an \, integer \tag{21}$$

So we see a natural length scale Δ developing for the filament - but we can do even better than Eq. (21). We can argue that the preferred Δ is in fact:

$$\Delta = L \, or \, mL \tag{22}$$

This is because to form a conformation with a Δ greater than L, it requires lifting a point already bonded to the surface. Since all bonded points are equally likely to be lifted, there

Soft Matter Accepted Manuscript

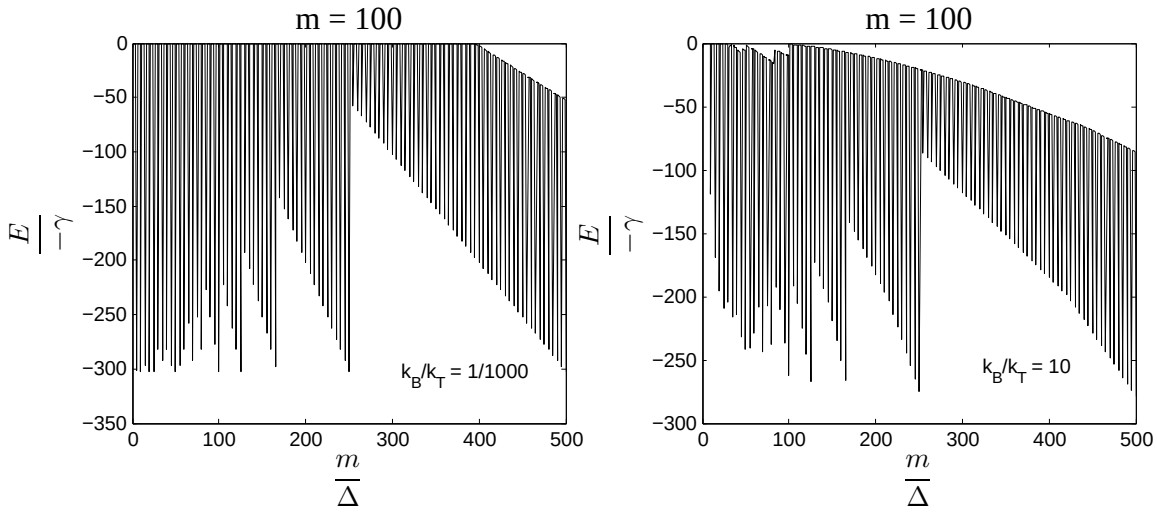

Figure 4: The conformation energy of the filament, Eq. (20), as a function of the periodicity, Δ. For each Δ, the plotted energy is also minimized with respect to the length of the bonding region δ. When $N\Delta = mL$ where N is an integer and mL is the total filament length, we find a local minimum energy configuration. On the left, for $\kappa_B/\kappa_T = 10^{-3}$, we find a degenerate set of minimum energies. On the right, for $\kappa_B/\kappa_T = 10$, we do not see similar degenerate configurations and the minimum energy solution is found only when $\Delta = mL$.

are multiple kinetic traps indicative of a frustrated system. Thus $\Delta = L$ is the most readily accessible configuration while $\Delta = mL$ maximizes bonding (again referencing the "unwound" conformation).

Figure 4 shows that when the bending modulus is much less than the twist modulus, there are no structures where $L < \Delta < mL$ that correspond to a significantly lower energy state than for $\Delta = L$. As the bending modulus increases, larger Δ configurations become preferred since the filament must bend by π radians no matter how small δ becomes. The energy barriers present in this landscape originate from choices of Δ for which most of the twisted regions of the filament do not coincide with where the binding pattern is in contact with the surface. For these cases, the filament strains and "straightens out" the binding pattern, but does not increase the binding energy. For many of these choices of Δ the no-strain solution with zero energy is the preferred conformation.

For the amyloid case, L represents the turn period for CF-PT and Δ represents the turn

Soft Matter Accepted Manuscript

period for PHF. As mentioned in the introduction, we know this value to be shared between the two filaments and so will focus on a discussion of structures corresponding to the length scale $\Delta = L$. For an arbitrary filament where the bend modulus is much larger than the twist modulus, the treatment below will remain relevant with the selection of a larger preferred Δ. We should also note at this time that the special "unwound" case ($\Delta = mL$) does correspond to a lower energy state than any structure of period $\Delta = L$ for certain values of κ_B and κ_T. We will keep this case in mind as we construct the energy landscape.

B. Filament Energy Landscape

Allowing the twist to be piecewise constant still produces an infinite number of possible filament configurations. Here we will investigate four simple filament configurations and calculate their equilibria. Two unbending configurations are considered - the original, "Flat" filament, and one that merely twists, "Twisted," on the surface to increase bonding character then reverses that twist to meet the boundary conditions. Two bending configurations are considered - "Looped" of accumulated twist 2π ($\left|\frac{d\theta_3}{ds}\right| \equiv \frac{2\pi}{L}$) and "Helix" introduced in the previous section ($\left|\frac{d\theta_i}{ds}\right|$ piecewise constant). The "Looped", "Helix", and "Twisted" conformations are all kinetically quenched with fixed linking number.

To find the minimum energy configuration, a single parameter is varied: for the Looped case, this is the radius of the loop; for the Twisted and Helix cases this is the bonding length, δ (note for convenience the parameter $\beta \equiv \frac{L\delta}{2\pi}$ is introduced in the description of the Helix). Also note that the parameter β remains in the equation for the Helix due to the fact that the energy for this conformation is minimized numerically. The Flat, unstrained filament, has zero energy. (See Appendix B for the calculations.)

$$\begin{aligned} E^{Looped} &= \gamma L + 2\pi\left[2\sqrt{-\gamma\kappa_B} + \kappa_T\left(\tfrac{2\pi}{L}\right)\right] & E^{Twisted} &= 4\pi\sqrt{-\gamma\kappa_T} - (2\pi)^2\tfrac{\kappa_T}{L} + \gamma L \\ E^{Helix}(\beta) &= \kappa_B\tfrac{(\beta+\pi)^2}{L\left(1-\frac{\beta}{2\pi}\right)} + \kappa_T\beta\tfrac{2\pi}{L} + \gamma\beta\tfrac{L}{2\pi} & E^{Flat} &= 0 \end{aligned} \tag{23}$$

A table containing a list of all parameters used to define the energies above and construct the phase diagram in Figure 6. is displayed below:

Before we move on, we would like to take a moment to discuss the physical nature of these parameters. κ_B and κ_T are mechanical properties of the filament representing their rigidity with respect to bending and twisting. γ depends on the nature of the binding between the

Soft Matter Accepted Manuscript

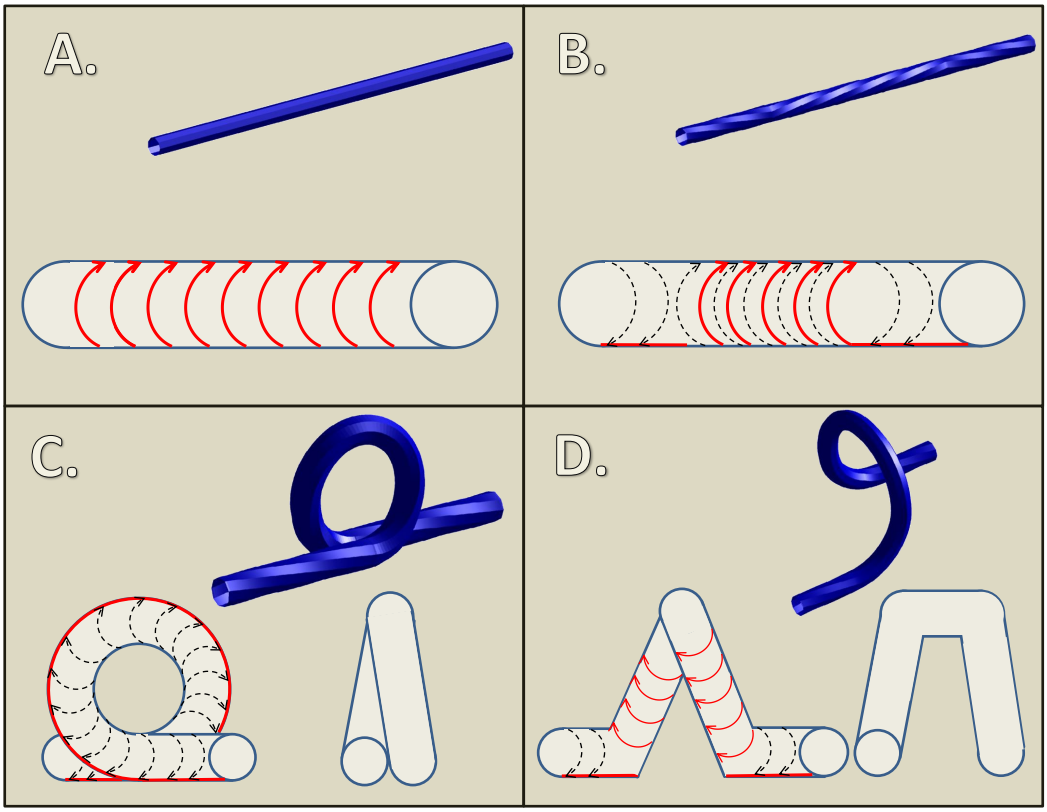

Figure 5: Pictures of the four calculated filament configurations with piecewise constant twist interacting with a flat surface.

surface and helical pattern of the filament: the more strongly binding, the more negative γ becomes. is the length of repeat for the helical pattern of the filament. Δ is the period for the filament conformation (e.g. the Looped period). δ is the length over which the filament twists and binds to the surface within each period Δ.

We may see that even after energy minimization with respect to β is completed, the above equations still contain four parameters; however, we may scale the energy by length and γ to return only two degrees of independence (the compound parameters $\frac{\kappa_B}{-\gamma L^2}$ and $\frac{\kappa_T}{-\gamma L^2}$).

$$\begin{aligned} \frac{E^{Looped}}{-\gamma L} &= 2\pi\left[2\sqrt{\frac{\kappa_B}{-\gamma L^2}}+2\pi\frac{\kappa_T}{-\gamma L^2}\right]-1 & \frac{E^{Twisted}}{-\gamma L} &= 2\pi\left[2\sqrt{\frac{\kappa_T}{-\gamma L^2}}-2\pi\frac{\kappa_T}{-\gamma L^2}\right]-1 \\ \frac{E^{Helix}(\beta)}{-\gamma L} &= \frac{\kappa_B}{-\gamma L^2}\frac{(\beta+\pi)^2}{\left(1-\frac{\beta}{2\pi}\right)}+\frac{\kappa_T}{-\gamma L^2}2\pi\beta+-\frac{\beta}{2\pi} & \frac{E^{Flat}}{-\gamma L} &= 0 \end{aligned} \tag{24}$$

The first thing we may notice from the equilibria with the untwisted states, is all three mechanically strained phases have the same maximum twisting modulus such that if it is above the critical value, the filament remains "flat" and does not strain to interact with the

Soft Matter Accepted Manuscript

Parameter	Meaning
κ_B	Bend Modulus
κ_T	Twist Modulus
γ	Surface Binding Character (Energy Density)
L	Filament Pattern Period
Δ	Filament Conformation Period
δ	Length of Binding Region Within Period
β	$\frac{L\delta}{2\pi}$

Table I: A summary of the key parameters used in this study. While it may be difficult to do so for some, all are measurable quantities.

surface for any bending modulus. Scaling in the same fashion as above:

$$\frac{\kappa_T^{critical}}{-\gamma L^2} = \left(\frac{1}{2\pi}\right)^2 \tag{25}$$

Similarly, we can generate a upper bound for the critical bending modulus beyond which the Twisted configuration is preferred. Taking the limiting case $\kappa_T = 0$:

$$\frac{E^{Helix}(\beta)}{-\gamma L} = \frac{\kappa_B}{-\gamma L^2}\frac{(\beta+\pi)^2}{\left(1-\frac{\beta}{2\pi}\right)} - \frac{\beta}{2\pi} \tag{26}$$

we have the following condition for the boundary between Helix and Flat:

$$E^{Helix}(\beta) = 0 \Leftrightarrow \frac{\kappa_B}{-\gamma L^2} = \frac{\beta\left(1-\frac{\beta}{2\pi}\right)}{2\pi\left(\beta+\pi\right)^2} \tag{27}$$

This function attains its maximum with respect to β when $\beta = \frac{\pi}{2}$ and in that substitution we get an upper bound for κ_B:

$$\frac{\kappa_B^{critical}}{-\gamma L^2} \leq \frac{1}{3}\left(\frac{1}{2\pi}\right)^2 \tag{28}$$

The phase diagram for the four configurations discussed above is shown in Figure 6. For any point where $\kappa_T < \kappa_T^{critical}$, we know the filament strains to interact with the surface. Further, for any point in this region where $\kappa_B > \kappa_B^{critical}$, the Twisted phase is preferred.

Let us finally return to consider the "unwound" case:

$$\frac{E^{unwound}}{m} = \frac{1}{m}\int_0^{mL} \kappa_T\left(\frac{2\pi}{L}\right)^2 + \gamma(1)ds \tag{29}$$

Soft Matter Accepted Manuscript

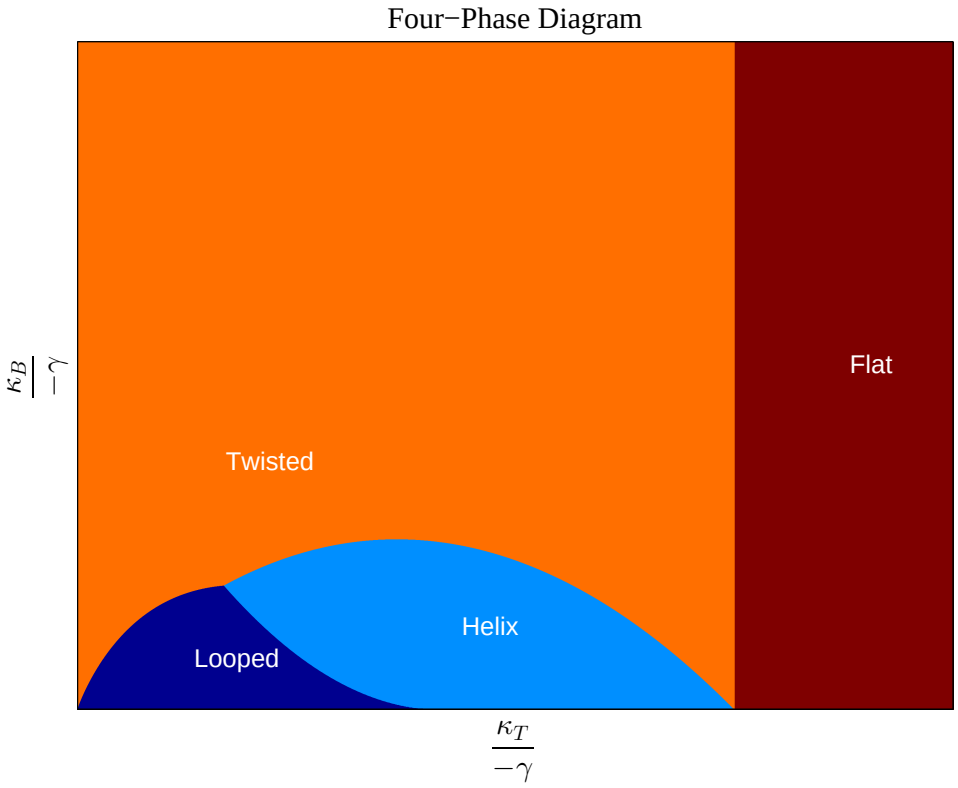

Figure 6: The phase diagram for the four filament configurations where the rightmost Flat configuration change occurs at $\frac{\kappa_T^{critical}}{-\gamma L^2} = \left(\frac{1}{2\pi}\right)^2$ and the upper limit for the y-axis is taken to be our upper bound for $\frac{\kappa_B^{critical}}{-\gamma L^2} \equiv \frac{1}{3}\left(\frac{1}{2\pi}\right)^2$. The "Looped", "Helix", and "Twisted" conformations are all kinetically-quenched with fixed linking number.

$$= L\left(\kappa_T\left(\frac{2\pi}{L}\right)^2 + \gamma\right) \tag{30}$$

We see that:

$$E^{unwound} = 0 \Rightarrow \frac{\kappa_T}{-\gamma L^2} = \left(\frac{1}{2\pi}\right)^2 \tag{31}$$

which is the critical point shared by all other mechanically strained phases. As mentioned earlier, this phase is lower energy than any other phase considered within this critical value of κ_T. It is the only conformation described in this work for which the linking number changes with strain. If the linking number changes, the other conformations examined here are predicted to destabilize and degenerate to this conformation; however relaxation of the linking number requires the propagation of twist directed from a single initial point of contact throughout the length of the entire filament and a suppression of twist originating from any

Soft Matter Accepted Manuscript

other point. In a statistically relevant ensemble there must be some distribution of this case, but it will be easy to distinguish from the other phases present as it will not appear curved.

C. Modeling the CF-PT to PHF transition

We have shown the existence of a helical secondary structure for a cylindrical filament with a helical bonding pattern. Now we want to show that this work is relevant for the CF-PT fibril as well. As displayed in Figure 1, CF-PT is a twisted triangular prism; thus each slice of the fibril has three potential bonding edges and these edges form three helices over the length of the fibril. In order to map this shape to our toy model, we first have to identify L, the period of the fibril. This is one third the period of the triple helix: the distance between slices where an edge is facing downward (in contact with the surface). See Figure 7.

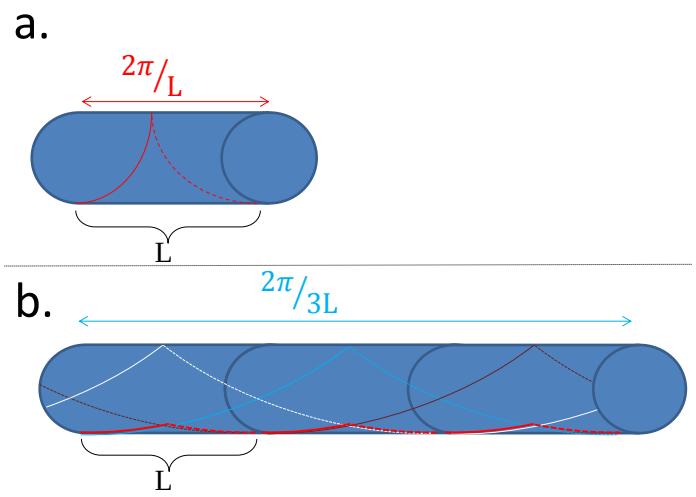

Figure 7: a. A single monomer of the original model: here the period of the pattern (rotation of 2π) is equal to the period of the single helix, L. b. Three monomers in the model corresponding to CF-PT: here the period of the pattern (L) is one third the period of the three helices. Note in b. the three helices are drawn in brown, white, and blue and the bonding pattern (comprising sections of each helix) is drawn in red.

Over this length, we can identify the edge in each slice closest to the surface and label it as the bonding edge. This leaves us with a bonding pattern which is the first sixth of

Soft Matter Accepted Manuscript

a helix of period $3L$ stitched together with the last sixth of such a helix. This shape is indistinguishable from our toy model when constructing the Helix secondary structure since that conformation does not twist or touch the surface in the center of each period. We may now return to our expression for the energy of the Helix conformation, identified as PHF. The only thing we must change is the bonding twist which was $\frac{2\pi}{L}$ for the toy model and is $\frac{2\pi}{3L}$ for the real fibril since the triple helix in the real fibril has period $3L$.

Returning to (23) and introducing the factor of $\frac{1}{3}$ yields:

$$E^{Helix}(\beta) = \kappa_B \frac{(\beta+\pi)^2}{L\left(1-\frac{3\beta}{2\pi}\right)} + \kappa_T \beta \frac{2\pi}{3L} + \gamma\beta\frac{3L}{2\pi} \tag{32}$$

with the critical points:

$$\kappa_T^{critical} = -\gamma\left(\frac{3L}{2\pi}\right)^2 \; and \; \kappa_B^{critical} = -\gamma\frac{3}{5}\left(\frac{L}{2\pi}\right)^2\left(1-\frac{\kappa_T}{-\gamma}\left(\frac{2\pi}{3L}\right)^2\right) \tag{33}$$

beyond which the Flat conformation is preferred. Allowing only this proposed PHF secondary structure for the fibril and identifying the Flat conformation as CF-PT we can construct a phase diagram as was done above for toy model (See Figure 8).

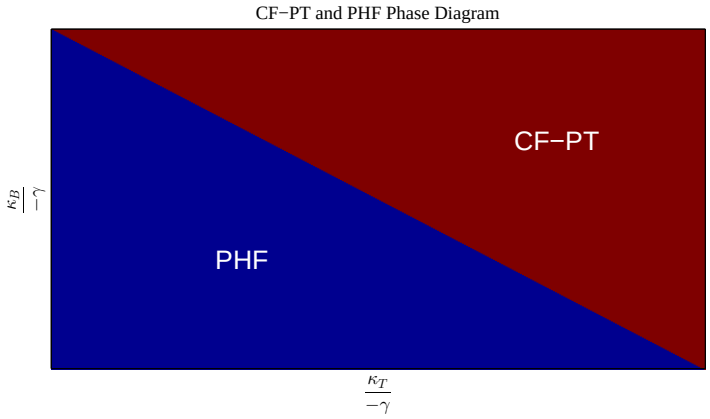

Figure 8: CF-PT and PHF phase diagram with the critical twist and bend moduli $\frac{\kappa_T^{critical}}{-\gamma} = \left(\frac{3L}{2\pi}\right)^2$ *and* $\frac{\kappa_B^{critical}}{-\gamma} \equiv \frac{3}{5}\left(\frac{L}{2\pi}\right)^2$ specifying the axis delimiters.

We can further illustrate the detail of the fibril periods by constructing them directly (through rigid body rotation and translation) from the atomic coordinates published online by Paravastu et al.[7] (PDB ID: 2LMP) in the Protein Data Bank[13] (www.rcsb.org). Shown below (in Figure 9) is the original PDB structure of the amyloid segment alongside three

Soft Matter Accepted Manuscript

fibrils of one period in length: CF-PT, PHF (described above), and modified PHF. The modified PHF structure is a higher energy conformation included for visual comparison with experimental images (see Figure 10); however, it should be noted that the associated bend energy is higher. The fibril may assume such a higher energy conformation with more tightly bent segments to reduce the movement of period endpoints during bending.

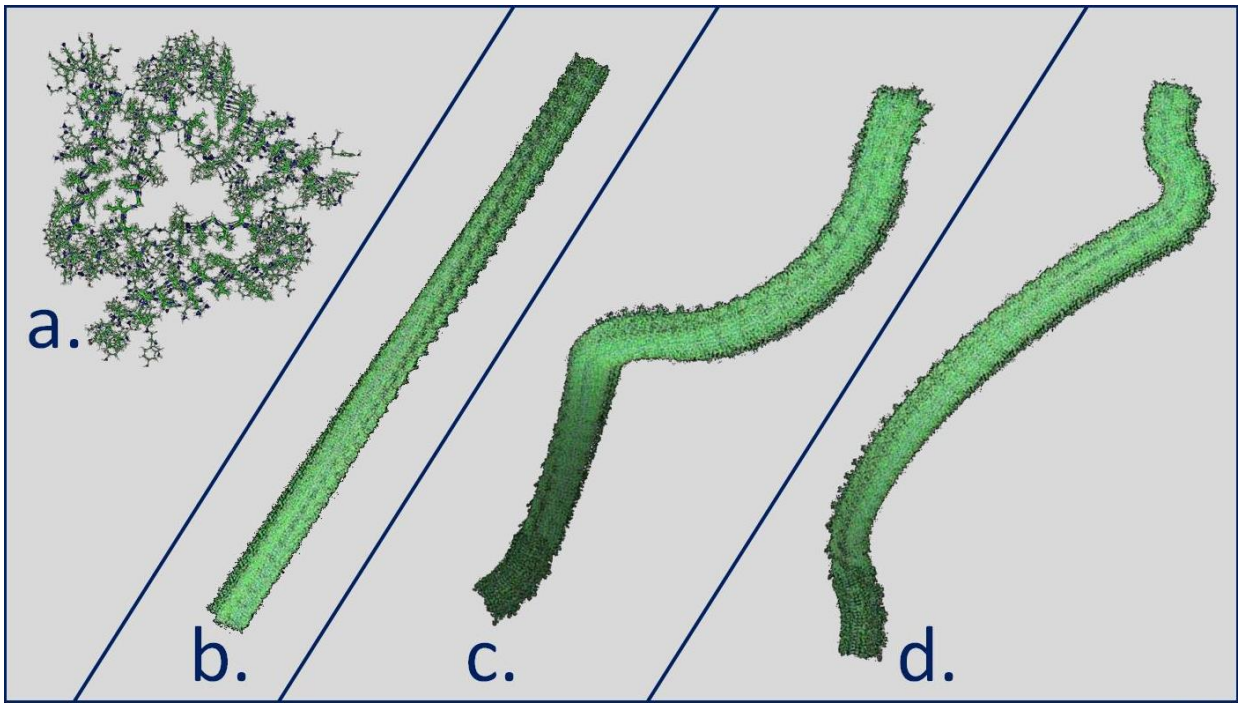

Figure 9: Molecular models of the fibril where: a. is the axial view of the fibril section published online (PDB ID: 2MLP), b. is a CF-PT monomer, c. is a PHF monomer, and d. is a modified PHF monomer with a higher associated bend energy but requiring less motion of the endpoints (when converting from CF-PT).

III. DISCUSSION

We have explored a variety of filament shapes possible for helically patterned elastic filaments binding to a surface, and provided a surface mediated mechanism for the conversion of CF-PT to PHF. Motivated by experimental images, we focused on writhing conformations for which the linking number remains fixed. When the linking number changes, all of the strained conformations explored here are predicted to degenerate into the "Unwound" case.

Soft Matter Accepted Manuscript

Below in Figure 10, we show a visual comparison between STEM images reprinted from Ruben et al.[5] and simplified versions of the molecular structures shown in Figure 9. The color in these images is due to the dye used in STEM: dye is placed on the surface and thus higher regions appear lighter in color. The simulated structures follow this convention.

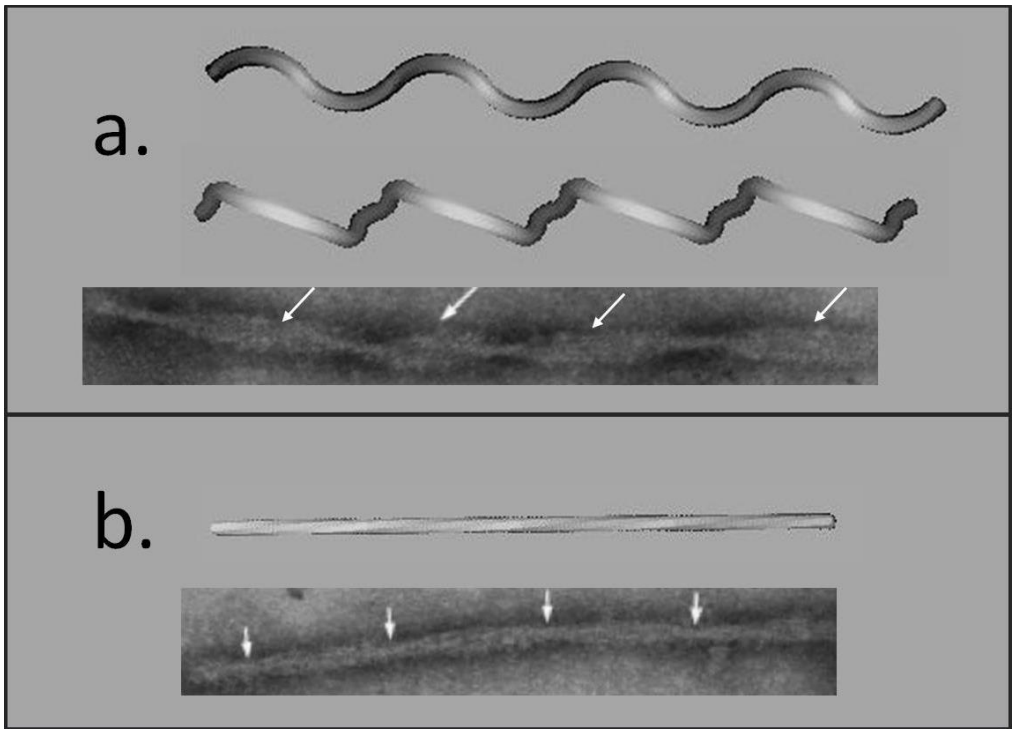

Figure 10: Visual comparison between experimental STEM images (reprinted from Ruben et al.[5]) and simplified versions of the molecular structures shown in Figure 9 colored to resemble the staining pattern of the STEM images: a. shows the PHF and modified PHF structures where the white arrows labelling the experimental image refer to the raised section of each period and b. shows the CF-PT where the arrows refer to the thin sections of each period.

Recent work coupling experiment and simulation-based image analysis [14] has provided evidence to suggest the untwisting of amyloid fibrils when they are membrane-bound. While it is yet unclear whether this untwisting observed is directly a CF-PT to PHF conversion, the work nonetheless motivates further consideration of amyloid fibril-membrane interactions that may forestall pathological aggregation. More generally, results of this paper suggest that helical filaments and their interaction with substrates can generate a variety of configurations. This is relevant for the microfabrication of devices constructed from a variety of materials (e.g. collagen[15] and other proteins[16], hydrogel[17], etc.) which allow for the

Soft Matter Accepted Manuscript

design of increasingly sophisticated systems (e.g. synthetic flagella[18]) from the directed or self assembly of nanoscale filaments. Recent theoretical work has complemented these experimental advances by predicting a variety of shapes that filament bundles may adopt depending on the relative values of the bend and twist moduli, and the nature of the filament-filament bonding interactions[19, 20]. Additionally, many cell cytoskeletal systems are composed of filament bundles (e.g. actin networks[21, 22], membrane traffic complexes[23], etc.) motivating work on the elucidation of intermediate filament structures[12] (e.g. CF-PT and PHF) and their, often nontrivial (e.g. fractal patterning[24]) organization. We hope that the work presented here will be useful both for microfabrication and the investigation of tau fibrils and other intermediate filament structures.

IV. APPENDIX

A. bend and twist equivalency

There is also one further consideration we must take into account: we must determine what types of bend are equivalent to twisting the filament. The basic problem statement is that we want to know what collections of rotations about $\mathbf{e}_1$ and $\mathbf{e}_2$ are equivalent to a single rotation about $\mathbf{e}_3$. Note that in the description below without a loss of generality $\mathbf{e}_1 = \mathbf{e}_x$ etc.). Stated another way, we want to know the requirements on angles a, b, and c such that a rotation about $\mathbf{e}_2$ by c, followed by a rotation about $\mathbf{e}_1$ by b, and then about $\mathbf{e}_2$ by a is equivalent to a rotation about $\mathbf{e}_3$ by d:

$$\begin{bmatrix} \cos(a) & 0 & -\sin(a) \\ 0 & 1 & 0 \\ \sin(a) & 0 & \cos(a) \end{bmatrix} \begin{bmatrix} 1 & 0 & 0 \\ 0 & \cos(b) & -\sin(b) \\ 0 & \sin(b) & \cos(b) \end{bmatrix} \begin{bmatrix} \cos(c) & 0 & -\sin(c) \\ 0 & 1 & 0 \\ \sin(c) & 0 & \cos(c) \end{bmatrix} = \begin{bmatrix} \cos(d) & -\sin(d) & 0 \\ \sin(d) & \cos(d) & 0 \\ 0 & 0 & 1 \end{bmatrix} \tag{34}$$

We discover the following relationships hold:

$$c = \frac{\pi}{2}, a = \frac{3\pi}{2}, b = -d \, or \, c = \frac{3\pi}{2}, a = \frac{\pi}{2}, b = d \tag{35}$$

In other words, any rotation about $\mathbf{e}_3$ can be achieved by moving the plane formed by $\mathbf{e}_1$ and $\mathbf{e}_2$ into the plane normal to $\mathbf{e}_3$ and rotating about $\mathbf{e}_1$ by an equivalent angle. Now let us verify that any arbitrary rotation may be written as a rotation about only two axes (i.e.

Soft Matter Accepted Manuscript

that combinations of bend deformations alone is equivalent to an arbitrary rotation of the local coordinate frame). Let $\mathbf{X}$,$\mathbf{Y}$, and $\mathbf{Z}$ represent rotation matrices about axes $\mathbf{e}_1$,$\mathbf{e}_2$, and $\mathbf{e}_3$ respectively. We begin with an arbitrary rotation of the form $\mathbf{ZXY}$. We can write this rotation as $\mathbf{ZXY} = \mathbf{Z}'\mathbf{Y}'^T\mathbf{X}'\mathbf{Y}''$ where $\mathbf{Y}'$ is a rotation of $\frac{\pi}{2}$ or $\frac{3\pi}{2}$ and $\mathbf{Z}'$, $\mathbf{X}'$ and $\mathbf{Y}''$ are arbitrary. Now we can rewrite $\mathbf{Z}'$ as a rotation about only $\mathbf{e}_1$ and $\mathbf{e}_2$ as $\mathbf{Z}' = \mathbf{Y}'\mathbf{X}''\mathbf{Y}'$ where $\mathbf{X}''$ is another rotation. We obtain $\mathbf{Z}'\mathbf{Y}'^T\mathbf{X}'\mathbf{Y}'' = (\mathbf{Y}'\mathbf{X}''\mathbf{Y}')\mathbf{Y}'^T\mathbf{X}'\mathbf{Y}'' = \mathbf{Y}'\mathbf{X}''\mathbf{X}'\mathbf{Y}'' = \mathbf{Y}'\mathbf{X}'''\mathbf{Y}''$. Thus we have verified that any arbitrary rotation can be decomposed into rotations about $\mathbf{e}_1$ and $\mathbf{e}_2$.

B. conformation energy minimization

To find the minimum energy for the three filament conformations considered ("Twisted", "Looped", and "Helix"), a single parameter is varied: for the Looped case, this is the radius of the loop; for the Twisted and Helix cases, this is the bonding length, δ. Let us begin with the purely twisted case. First, divide the filament into two sections. One with twist of $2\pi/L$ over length δ and a second of negative twist over the nonbonding region $L-\delta$ to ensure that a null rotation is achieved from end to end. Labelling these regions A and B, we have

$$\frac{\partial\theta_3^A}{\partial s} = \frac{2\pi}{L} \tag{36}$$

$$\frac{\partial\theta_3^B}{\partial s} = \frac{\frac{2\pi}{L}\delta}{L-\delta} = \frac{2\pi}{L}\left[\frac{\delta}{L-\delta}\right] \tag{37}$$

$$\Rightarrow E^{Twisted} = \kappa_T\left(\frac{2\pi}{L}\right)^2\delta\left[1+\frac{\delta}{L-\delta}\right] + \gamma L \tag{38}$$

with the preferred δ value that corresponds to the lowest energy:

$$\delta^* = L\left[1-\frac{2\pi}{L}\sqrt{\frac{\kappa_T}{-\gamma}}\right] \tag{39}$$

This yields a minimum energy of the Twisted configuration:

$$\Rightarrow E^{Twisted} = 4\pi\sqrt{-\gamma\kappa_T} - (2\pi)^2\frac{\kappa_T}{L} + \gamma L \tag{40}$$

With this we can find the line of coexistence with the untwisted Flat configuration (null energy):

$$E^{Flat} = E^{Twisted} \Leftrightarrow \frac{\kappa_T}{-\gamma} = \frac{L^2}{4\pi^2} \tag{41}$$

Soft Matter Accepted Manuscript

Now let us investigate the Looped configuration. The filament length is given by:

$$L = 2\delta + 2\pi R \tag{42}$$

where δ again is the length of each bonding region, and R is the radius of the circular portion. This yields for bonding energy: $E_{bond} = \gamma(L - 2\pi R)$. To calculate the bending energy we first note that the curvature is constant around the circular portion of the curve and zero elsewhere, yielding:

$$\frac{d\theta_2}{ds} = \frac{2\pi}{2\pi R} = \frac{1}{R} \tag{43}$$

Therefore the bending energy is

$$E_{bend} = \kappa_B \frac{2\pi}{R} \tag{44}$$

The twist energy is the same as for the Twisted case above:

$$E_{twist} = \kappa_T \frac{(2\pi)^2}{L} \tag{45}$$

which leads to a total energy of:

$$E^{Looped} = E_{bend} + E_{twist} + E_{bond} = \kappa_B \frac{2\pi}{R} + \kappa_T \frac{(2\pi)^2}{L} + \gamma(L - 2\pi R) \tag{46}$$

and a preferred R corresponding to the minimum energy solution:

$$R^* = \sqrt{\frac{\kappa_B}{-\gamma}} \tag{47}$$

which yields:

$$E^{Looped} = \gamma L + 2\pi \left[2\sqrt{-\gamma \kappa_B} + \kappa_T (\frac{2\pi}{L}) \right] \tag{48}$$

As before, we can find the line of coexistence with the untwisted configuration (null energy):

$$E^{Looped} = E^{Flat} \Leftrightarrow \frac{\kappa_B}{-\gamma} = \left(\frac{L}{4\pi} - \frac{\pi}{L} \frac{\kappa_T}{-\gamma} \right)^2 \tag{49}$$

For the Helix case we can begin by rewriting Eq. (17) for a single period where $\Delta = L$:

$$E^{L,\delta} = \frac{\kappa_B}{L - \delta} \left(\frac{2\pi\delta}{L} + \pi \right)^2 + \kappa_T \delta \left(\frac{2\pi}{L} \right)^2 + \gamma\delta \tag{50}$$

identifying $\beta = \frac{L\delta}{2\pi}$:

$$E^{Helix}(\beta) = \kappa_B \frac{(\beta + \pi)^2}{L\left(1 - \frac{\beta}{2\pi}\right)} + \kappa_T \beta \frac{2\pi}{L} + \gamma\beta \frac{L}{2\pi} \tag{51}$$

Soft Matter Accepted Manuscript

We will calculate the preferred β (and thus the minimum energy) numerically; however, we can note right away that for all values of β:

$$min\left(E^{Helix}(\beta)\right) \geq 0 \, for \, \kappa_T \geq -\gamma\left(\frac{L}{2\pi}\right)^2 \tag{52}$$

Restated, the energy of each configuration is as follows:

$$\begin{aligned} E^{Looped} &= \gamma L + 2\pi\left[2\sqrt{-\gamma\kappa_B} + \kappa_T\left(\tfrac{2\pi}{L}\right)\right] & E^{Twisted} &= 4\pi\sqrt{-\gamma\kappa_T} - (2\pi)^2\tfrac{\kappa_T}{L} + \gamma L \\ E^{Helix}(\beta) &= \kappa_B\tfrac{(\beta+\pi)^2}{L\left(1-\frac{\beta}{2\pi}\right)} + \kappa_T\beta\tfrac{2\pi}{L} + \gamma\beta\tfrac{L}{2\pi} & E^{Flat} &= 0 \end{aligned} \tag{53}$$

V. REFERENCES

[1] V. M. Lee, M. Goedert and J. Q. Trojanowski, *Annual review of neuroscience*, 2001, **24**, 1121–1159.

[2] R. A. Stelzmann, H. Norman Schnitzlein and F. Reed Murtagh, *Clinical anatomy*, 1995, **8**, 429–431.

[3] C. Goldsbury, U. Baxa, M. N. Simon, A. C. Steven, A. Engel, J. S. Wall, U. Aebi and S. A. Müller, *Journal of structural biology*, 2011, **173**, 1–13.

[4] M. Kidd, *Nature*, 1963, **197**, 192–193.

[5] G. C. Ruben, J.-z. Wang, K. Iqbal and I. Grundke-Iqbal, *Microscopy research and technique*, 2005, **67**, 175–195.

[6] G. Ramachandran and J. B. Udgaonkar, *Biochemistry*, 2013, **52**, 4107–4126.

[7] A. K. Paravastu, R. D. Leapman, W.-M. Yau and R. Tycko, *Proceedings of the National Academy of Sciences*, 2008, **105**, 18349–18354.

[8] D. A. Quint, A. Gopinathan and G. M. Grason, *Soft Matter*, 2012, **8**, 9460–9468.

[9] J. M. Mason and K. M. Arndt, *ChemBioChem*, 2004, **5**, 170–176.

[10] C. W. Wolgemuth and S. X. Sun, *Physical review letters*, 2006, **97**, 248101.

[11] O. N. Yogurtcu, C. W. Wolgemuth and S. X. Sun, *Biophysical journal*, 2010, **99**, 3895–3904.

[12] S. Köster, D. A. Weitz, R. D. Goldman, U. Aebi and H. Herrmann, *Current opinion in cell biology*, 2015, **32**, 82–91.

[13] H. M. Berman, J. Westbrook, Z. Feng, G. Gilliland, T. Bhat, H. Weissig, I. N. Shindyalov and P. E. Bourne, *Nucleic acids research*, 2000, **28**, 235–242.

Soft Matter Accepted Manuscript

[14] G. Gorbenko, V. Trusova, M. Girych, E. Adachi, C. Mizuguchi, K. Akaji and H. Saito, *Soft matter*, 2015, **11**, 6223–6234.

[15] K.-H. Shin, J.-W. Kim, Y.-H. Koh and H.-E. Kim, *Materials Letters*, 2015, **143**, 265–268.

[16] H. Dong, S. E. Paramonov and J. D. Hartgerink, *Journal of the American Chemical Society*, 2008, **130**, 13691–13695.

[17] S. Zhang, D. M. Marini, W. Hwang and S. Santoso, *Current opinion in chemical biology*, 2002, **6**, 865–871.

[18] B. J. Williams, S. V. Anand, J. Rajagopalan, M. T. Saif *et al.*, Micro Electro Mechanical Systems (MEMS), 2014 IEEE 27th International Conference on, 2014, pp. 192–195.

[19] I. R. Bruss and G. M. Grason, *Proceedings of the National Academy of Sciences*, 2012, **109**, 10781–10786.

[20] I. R. Bruss and G. M. Grason, *Soft Matter*, 2013, **9**, 8327–8345.

[21] M. Enrique and M. L. Gardel, *Journal of Biological Chemistry*, 2015, jbc–R115.

[22] S. X. Sun and H. Jiang, *Microbiology and Molecular Biology Reviews*, 2011, **75**, 543–565.

[23] A. K. Gillingham and S. Munro, *Biochimica et Biophysica Acta (BBA)-Molecular Cell Research*, 2003, **1641**, 71–85.

[24] A. Lomander, W. Hwang and S. Zhang, *Nano letters*, 2005, **5**, 1255–1260.

Soft Matter Accepted Manuscript

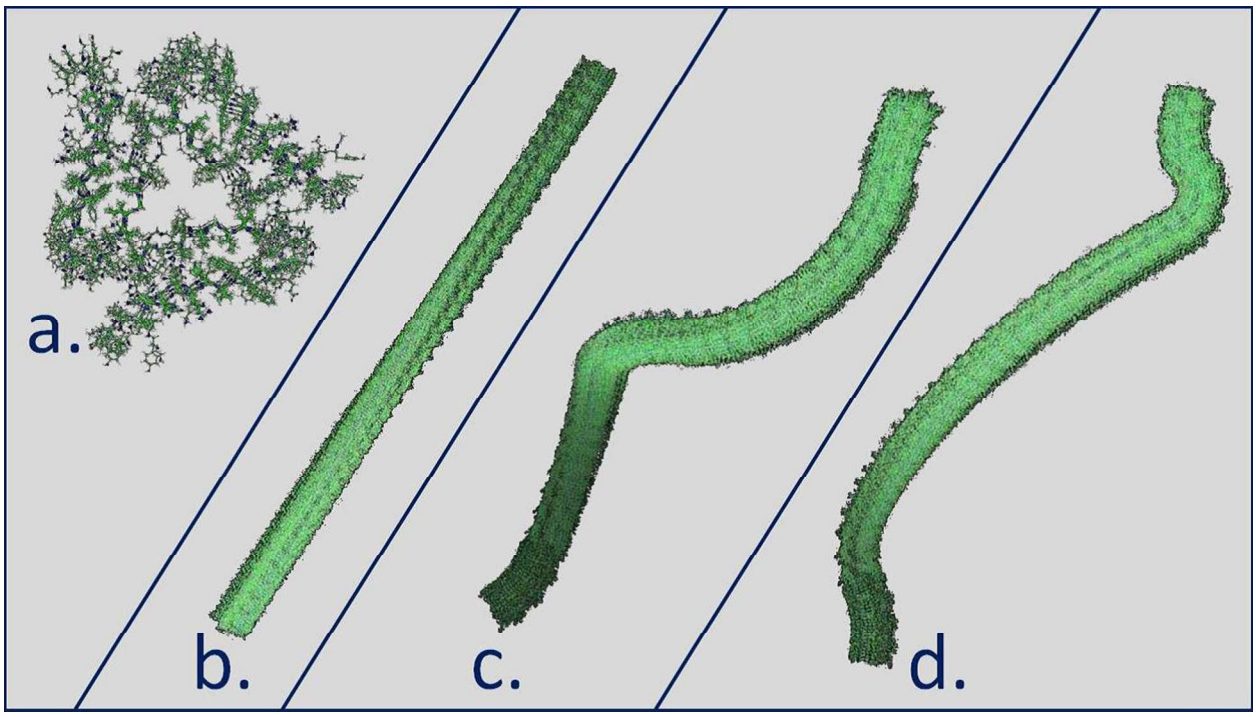

Here we provide a mechanistic explanation for the conversion of CF-PT amyloid fibrils (b.; a. cross-section) to PHF amyloid fibrils (c. and d.) thought to be important in the aggregation of pathological neurofibrillary tangles characteristic of Alzheimer's disease.

Soft Matter Accepted Manuscript